

The valuation of microstructural evolution in a thermo-mechanically processed TRansformation-TWinning Induced Plasticity steel during strain hardening

H. Eskandari Sabzi, A. Zarei-Hanzaki, A. Kaijalainen, A. Kisko



PII: S0921-5093(18)31274-7
DOI: <https://doi.org/10.1016/j.msea.2018.09.068>
Reference: MSA36949

To appear in: *Materials Science & Engineering A*

Received date: 10 July 2018
Revised date: 18 September 2018
Accepted date: 19 September 2018

Cite this article as: H. Eskandari Sabzi, A. Zarei-Hanzaki, A. Kaijalainen and A. Kisko, The valuation of microstructural evolution in a thermo-mechanically processed TRansformation-TWinning Induced Plasticity steel during strain hardening, *Materials Science & Engineering A*, <https://doi.org/10.1016/j.msea.2018.09.068>

This is a PDF file of an unedited manuscript that has been accepted for publication. As a service to our customers we are providing this early version of the manuscript. The manuscript will undergo copyediting, typesetting, and review of the resulting galley proof before it is published in its final citable form. Please note that during the production process errors may be discovered which could affect the content, and all legal disclaimers that apply to the journal pertain.

The valuation of microstructural evolution in a thermo-mechanically processed TRansformation-TWinning Induced Plasticity steel during strain hardening

H. Eskandari Sabzi¹, A. Zarei-Hanzaki^{1*}, A. Kaijalainen², A. Kisko²

¹Hot Deformation & Thermomechanical Processing of High Performance Engineering Materials Lab, School of Metallurgy and Materials Engineering, College of Engineering, University of Tehran, Tehran, Iran

²Materials and Production Engineering, Centre for Advanced Steels Research, University of Oulu, Oulu, Finland

* Corresponding author, e-mail: zareih@ut.ac.ir

Abstract

The successive evolution of martensitic transformation, twinning and dislocation substructure formation in a transformation-twinning induced plasticity steel during room temperature straining was studied in the present work. This was materialized through microstructural observations and micro-texture examinations utilizing the electron backscattered diffraction method. To evaluate the strain hardening behaviour of the thermomechanically processed steel, tensile testing procedure to different strains at ambient temperature was practiced. The results indicated that the dislocation slip, mechanical twinning, and deformation induced ϵ/α' -martensite formation were involved as the deformation mechanisms. At the early stages of deformation, the dynamic formation of dislocation substructure, strain induced ϵ -martensite and twins from austenite played the main role in the observed work hardening behavior. Furthermore, the results demonstrated that the formation of α' -martensite was the dominant deformation mechanism at higher deformation levels. The corresponding texture analysis indicated to a double fibre texture formation, with a relatively stronger $\langle 111 \rangle$ at lower strains and a stronger $\langle 100 \rangle$ partial fibre parallel to tensile axis at higher strains. However, in the latter, the Cube, A and Goss Twin (GT)-type textures were dominated. Decreasing of the Goss and S components were attributed to the preferential transformation of austenite to α' - and ϵ -martensites, respectively. The presence of GT component even at higher strains approved the participation of deformation induced twinning as a dominant deformation mechanism up to failure.

Keywords:

Transformation-twinning induced plasticity steel; dislocation; deformation twins; martensitic transformation; α' -martensite; texture evolution

1. Introduction

The strategy of enhancing the mechanical properties of any steel is strongly dependent upon its composition. For instance, during plastic deformation of metastable austenite, this phase, depending upon its composition thereby its stacking fault energy, may decompose partially into either ϵ - and/or α' -martensite in the so-called TRIP (TRAnsformation Induced Plasticity) and/or exhibit TWIP (TWinning Induced Plasticity) effects. These are competing deformation mechanisms and would markedly increase the strain hardening rate, strength and ductility [1-4]. In fact, the strain induced martensite formation and the mechanical twinning are kicked off to accommodate the undertaken additional strain. Furthermore, the stacking fault energy (SFE) dictate the ease of dislocation cross slip thereby allowing different deformation mechanisms to be activated at different stages of deformation [3,4]. Decreasing the SFE may lead to the larger stacking fault regions and this in turn would make the dislocation cross slip becoming more difficult. The latter is believed to favour the mechanical twinning during straining. In fact, those steels holding low to moderate SFE tend to form extended stacking faults, deformation twins and planar dislocation structures [4]. These different lattice defects strongly influence the steel flow behaviour and the evolution of texture during cold working. In addition, the transformation of austenite into martensite can be induced by plastic deformation in these steels [5–7]. During cold deformation, the austenite phase may partially transform to α' -martensite and the remaining austenite would be deformed by slip or deformation twinning [8]. It has been reported that the aforementioned stacking fault based microstructural evolutions may be simultaneously activated

to play important roles during deformation if the SFE would be valued between 15 and 20 mJ/m² [9].

As is well established, the deformation twinning can be considered as a nucleation and growth process [10]. Twin growth is expected to advance by co-operative movement of Shockley partials on subsequent {111} planes. The possible mechanisms to furnish this co-operative movement are the pole mechanism [11], a cross slip mechanism [12] or the interaction between primary and secondary slip systems [5]. Alternatively, nucleation of deformation twins contains the formation of required dislocation structures for the further twin growth [13,14]. Dislocation slip is therefore a prerequisite for twin formation.

Variant selection and strain accommodation are the two main mechanisms for TRIP effect [15,16]. Strain accommodation mechanism means that load transfer can be occurred from strain induced martensite which is harder than the austenite matrix. Variant selection is the main strain accommodation mechanism during deformation of full austenitic high Mn steels. In these steels, martensitic transformation can be influenced by the initial texture of austenite. Kireeva and Chumlyakov found the relationship between the austenite texture and the kinetics of martensitic transformation. They also showed that high amounts of ductility in TRIP steels can be attributed to the interactions between twinning, martensitic transformation and shear banding [17]. According to their texture studies [17], the <110> orientations in austenite were not suitable orientations for getting the highest elongations during tensile testing. In other studies, researchers [18,19] observed that grains with <111> parallel to the rolling orientations have much more potential for strain induced transformations in comparison with the <100> directions in cold rolled stainless steels. Based on these results, they quantified the martensitic transformation potential and therefore, the significance of austenite texture was revealed. Zhang et al. [20]

showed that martensite can be formed in grains with Cube and Goss orientation during tensile testing. Despite the valuable researches which have done recently on the influence of texture on the extent and the kinetics of martensitic transformation, the theoretical predictions are not always in agreement with the experimental results. The presence of ϵ -martensite phase and deformation twins also further complicates the situation. Based on the matters above, the orientation dependence of the martensitic transformation in polycrystalline austenite, where two types of martensite and deformation twins may present, is not so clear and requires further detailed studies.

The texture evolutions in FCC materials are well established based on SFE. In high and medium SFE materials, the Cu-type texture comprising the Cu, S and Brass components can be formed during cold deformation. Whereas, the α -brass type texture comprising predominantly the Brass and Goss components would be the main texture of the low SFE materials such as high Mn austenitic steels during room temperature deformation [42,43].

In the present investigation, a TRIP-TWIP steel composing of Fe-21Mn-1.6Al-2.5Si-0.1C was considered. In this steel, the formation of ϵ - and α' -martensite and twinning during deformation have been already reported (SFE ~ 18 mJ/m² [22]). It has frequently been observed that hexagonal ϵ and twinning act as an intermediate stage in the transformation from austenite to BCC α' -martensite [22]. This was reasoned based on the fact that the formation and evolution of ϵ and mechanical twins were dictated by similar mechanisms [20]. It is worth noting that the α' -martensite formation may also be strongly influenced by the steel SFE [23].

One important aspect of TRIP steels that has not been considered in details, is the role of crystal orientation or texture. The latter is expected to influence the stimulation of deformation induced martensite formation as well as the state of produced martensite phase. Some limited

results on the effect of textures in rolled alloys have been presented by Bracke et al. [24] and by Li et al. [25]. The occurrence of mechanical twinning in certain FCC alloys is well believed to be intimately associated with certain texture components [27,28]. It may be expected that some similar behaviour would take place in steels where ϵ - and α' -martensite formed simultaneously with mechanical twinning during deformation. These are some of the important issues which were initially considered to investigate in the present work.

As is well established [15], the uniaxial tensile deformation of FCC materials may result in the development of a $\langle 111 \rangle$ and $\langle 100 \rangle$ double fibre texture parallel to the loading axis. The relative volume fraction of the two fibres is generally dependent on the value of the material's SFE. Following to English and Chin [28], for intermediate to low SFE materials, the volume fraction of the $\langle 100 \rangle$ fibre is believed to be gradually increased by lowering the SFE values. The increase in the fraction of the $\langle 100 \rangle$ fibre is thought to be associated with a volume effect of deformation twinning wherein the $\langle 111 \rangle$ orientations can be reoriented by twinning to the intermediate $\langle 115 \rangle$ orientation. The $\langle 115 \rangle$ orientations subsequently may be rotated by slip towards the $\langle 100 \rangle$ orientation [29]. However, Stout et al. [30] argued that the increase in the fraction of the $\langle 100 \rangle$ fibre was probably due to the presence of a strong initial texture.

Considering all above, the present work was conducted to clarify the effects of parent austenite initial texture on the sequential formation of deformation twins and martensitic transformations as well as their effects on the rate of steel strain hardening and the involved deformation mechanisms. In addition, the effects of martensitic transformations, deformation twins and dislocation substructures evolutions on the texture development during tension are also discussed.

2. Experimental procedure

The chemical composition of experimented TRIP-TWIP steel in this study was certified as Fe-21Mn-1.6Al-2.5Si-0.1C. The experimental steel was received in as-cast condition. The as-cast material was first homogenized at 1180°C for 8 hours under a protective atmosphere. This was followed by rolling to total strain of 1.5 through 5 passes with the start and finishing temperatures of 1200/1000°C as the first cycle of thermomechanical processing (TMP) to break the dendritic structure of casting material. This was followed by instant quenching the thermomechanically processed (TMPed 1) material in water. Then the TMPed 1 workpieces were purposefully subjected to the second TMP cycle. This comprised of rolling the TMPed 1 workpieces down to the 30% thickness reduction at 1100°C through 1 pass followed by cooling them in the air. The hot rolled microstructure after the second TMP cycle (TMPed 2 sheets) consisted of a fully metastable austenite phase holding an average grain size of $23 \pm 7 \mu\text{m}$.

To evaluate the effects of initial state of austenite (e.g., grain size and texture) on the deformation behaviour of the experimental steel, tensile tests were carried out at room temperature under initial strain rate of 0.001 s^{-1} up to fracture. In addition, a set of interrupted tensile tests to logarithmic strains of $\epsilon = 0.15, 0.25, 0.35$ and 0.4 were performed to study the microstructural evolution as a function of strain. The tensile specimens were cut based on ASTM E8M standard [31] along the rolling direction (RD) from TMPed 2 sheets.

The microstructures of TMPed 2 TRIP-TWIP experimental steel after tensile deformation were examined by electron backscatter diffraction (EBSD) analysing method. The EBSD technique was used to analyse the local crystallographic texture together with martensitic transformations, deformation twinning and dislocation substructure. For the EBSD examinations, the specimen surfaces were first polished with a diamond suspension down to $1 \mu\text{m}$ and then

chemically polished using a 0.05 μm colloidal silica suspension. The EBSD measurements and analyses were performed using the EDAX-OIM acquisition and analysis software. The FESEM (Sigma, Zeiss) for the EBSD measurements was carried out at 15 kV with a step size of 0.50 μm .

3. Results

3.1. Strain hardening

The uniaxial tensile flow behaviour of the studied TMPed 2 TRIP-TWIP steel under initial strain rate of 0.001s^{-1} is illustrated in **Fig. 1a**. The material exhibits excellent mechanical properties, comprising high strength (ultimate tensile strength of 1.2 GPa) and desired ductility (elongation to failure of 50%). The marks on the curve indicate the corresponding points of interrupted tests at different strains.

As is seen in **Fig. 1b**, the variation of strain hardening rate with logarithmic strain follows four different stages. These will be described in the subsequent section. The main features in **Fig. 1b** are as follows: (i) the observed remarkable high overall strain hardening rate, and (ii) the fact that the curve reveals a minimum at intermediate strains (0.18-0.25). This hardening stage is followed by a high strain hardening rate at higher deformations. Typically, the structural metallic alloys reveal a monotonous decay of the strain hardening rate as a function of strain. However, as was seen, the present TWIP-TRIP steel exhibits four different deformation stages.

3.2. Microstructural evolution upon deformation

3.2.1. Martensitic transformations

The evolution of the martensitic transformations in tensile tested specimens were investigated by EBSD at four deformation stages corresponding to interrupted strain levels of

0.15, 0.25, 0.35 and 0.4. The qualitative information on the evolution of phases were generated through EBSD examinations and are shown in **Fig. 2**. In its initial hot rolled state (TMPed 2 condition) the material represented a fully austenitic structure, but this was not remained stable during deformation at room temperature. The ϵ - and α' -martensites were detected by EBSD in the microstructures of the tensile deformed specimens. **Fig. 2** also illustrates the phase and third nearest-neighbour kernel average misorientation (KAM) maps of the specimens with different interrupted strain levels. The corresponding phase fractions are summarized in **Table 1**. By increasing the tensile strain from 0 to 15%, the fraction of ϵ - and α' -martensites were increased from 0 to 17% and 3%, respectively (**Fig. 2a and b**). In addition, as are seen in the corresponding KAM maps (**Fig. 2f and 2g**), the KAM values were increased throughout the early uniform deformation regime, preferentially at the vicinity of internal interfaces and adjacent to the austenite phase regions. This, in line with the previous findings [25], suggests that the plastic strain and the lattice rotation were constructively accommodated inside the austenite. This trend of phase fractions behaviour is maintained upon further tensile deformation to 25%. In the latter stage, the average fraction of ϵ - and α' -martensites were reached to 27% and 7%, respectively (**Fig. 2c and Table 1**). The corresponding KAM maps reveal an increase in average misorientation throughout the microstructure; this suggests that a larger portion of the microstructure has contributed in accommodating the plastic deformation (**Fig. 2h**).

By further increasing the interruption tensile strain level from 25% to 35%, the average fraction of ϵ - and α' -martensites were increased to 36% and 21%, respectively (**Fig. 2d and Table 1**). The KAM map in **Fig. 2i** shows negligible increase in misorientation, with only a few regions holding a relatively low KAM value in the map.

At 40% tensile strain, almost 30% of FCC phase has been retained and the amount of ϵ -martensite is decreased to 25%, whereas the value of α' -martensite is raised to 45% (**Fig. 2e** and **Table 1**). As is seen in **Fig. 2j**, the KAM values have not undergone significant changes and a large portion of the microstructure contributed in accommodating the applied plastic strain.

3.2.2. *Twin and dislocation substructure*

The image quality (IQ), band contrast (BC) and the grain boundary (GB) maps were considered to track any microstructural evolutions in tensile deformed specimens (**Fig. 3**). The initial microstructure is characterized by an equiaxed grain type structure (where the twin boundaries are not considered, **Fig. 3a**). At 15% logarithmic strain level (**Fig. 3b**), striations in the form of parallel and intersected packets are evolved. These striations are nucleated mostly at the grain boundaries and are being bridged within the grains. By increasing the strain, the volume fraction of high angle grain boundaries is monotonically increased. A high fraction of deformation twin boundaries is seen in the tensile deformed specimens (**Fig. 4**). As is observed in **Fig. 4a**, most of the deformation bands are detected as deformation twin boundaries. Furthermore, The density of high angle twin boundaries appears to be progressively reduced by increasing the tensile strain. These twin boundaries locally present either as primary twins or as intersecting secondary ones. By further straining, the density of deformation twins seems to be decreased. The black lines in the **Fig. 4** are undetected areas, thereby not being considered as twin boundaries. This is attributed to the rotation of twin boundaries due to straining. Accordingly, all the twin boundaries in the highly strained microstructures cannot be detected through EBSD analysis. It is worth mentioning that the higher frequency of low and moderate angle grain boundaries, which are seen in **Fig. 3a** and **Fig. 5a**, is related to the restoration

processes during the applied TMP. The restoration processes appear to be preferentially taken place in grains with orientations close to $\langle 111 \rangle$ and $\langle 001 \rangle$ (**Fig. 6**, please see section 3.3)

The variation of misorientation angle distribution with tensile strain is shown in **Fig. 5**. The high fraction of deformation twins returns to the peaks at about 55° - 62° of the misorientation distribution histogram (**Fig. 5**). By applying tensile strain and in conjunction with the formation of high angle grain boundaries (**Fig. 3b-e**), the area fraction of low and moderate angle grain boundaries is decreased and being remained almost constant by increasing the tensile strain, with a decrease in twin boundaries (**Fig. 4a-d**). Reducing the twin boundaries population by increasing the tensile strain can be attributed to the undergoing martensitic transformation such that the twin/matrix misorientation relationship is progressively weakened as a result of increasing the necessitated local lattice rotations for maintaining the strain compatibility [33]. The deviation from the exact $60^\circ \langle 111 \rangle$ relationship is increased by intensifying the tensile strain up to the point that it exceeds the employed tolerance limit of 6° (following the Palumbo-Aust criterion). Hence, such boundaries are no longer identified as twin boundaries but are rather recognized as regular high angle grain boundaries [32].

3.3. Texture evolution

Fig. 6 shows the texture evolution of the TRIP-TWIP steel during tensile deformation. The initial microstructure (TMPed 2 one) reveals a strong texture (**Fig. 6a**). The evolution of texture in terms of TA-IPFs of the experimental TMPed 2 steel deformed to 0.15, 0.25, 0.35 and 0.4 logarithmic strains are given in **Fig. 6b-e**, respectively. As is seen, the texture is being slightly sharpened during tensile deformation. After tensile testing, the texture is characterized by two strong components, namely $\langle 111 \rangle$ /TA and $\langle 001 \rangle$ /TA, which both are remained stable and slightly sharpened during further straining. Nonetheless at lower strains,

the dominating texture is being $\langle 111 \rangle$ /TA component. By further straining, the intensity of $\langle 001 \rangle$ /TA component is increased through consuming the components between $\langle 111 \rangle$ and $\langle 001 \rangle$.

The evolutions of macro-texture components in the bulk experimental by increasing the tensile strain are given in **Fig. 7**. The ideal texture components of FCC materials and Schmidt factors (calculated for some of texture components) are shown schematically for $\phi_2 = 0^\circ$, 45° and 65° ODF sections in **Fig. 8** and **Table 2**.

The occurrence of partial recrystallization after hot rolling (TMPed 2 material) is characterized by a strong texture holding a maximum intensity of 17.75 (**Fig. 7a**). As is generally typical in FCC materials, the applied uniaxial tension has resulted in developing of the characteristic $\langle 111 \rangle$ and $\langle 001 \rangle$ double fibre texture parallel to the loading axis. At 25% tensile strain the maximum intensity lies on the $\langle 111 \rangle$ fibre in comparison with $\langle 001 \rangle$ fibre and then again it is continued as it was in the past (**Fig. 7b-e**). As is seen in **Fig. 7a**, the starting texture comprises of a rotated Cu (Rt-Cu) as the main component and a relatively weak Goss component. Both of these components are carried over from the applied TMP 2 hot rolling cycle.

By increasing the tensile strain to 15%, a pronounced increase in the intensity of the Goss and S components and a slight increase in G/B, Brass and GT (Goss Twin) is seen; this is associated with a concurrent disappearing of the Rt-Cu component (**Fig. 7b**). The GT and S components are the main texture components of the 25% tensile strain as a result of decrease in Goss component intensity; this is clearly seen in **Fig. 7c**. A slight amount of A component is also seen in this strain level. As is illustrated in **Fig. 7d**, by increasing the tensile strain up to 35%, the Cube component with maximum intensity of 20.71 is appeared. The Goss and A

components are being increased a bit and GT and S components are being decreased gradually. Finally, at 40% tensile strain, the Cube component is completely disappeared and the Goss, G/B, A and GT components are increased with a maximum intensity of 12.41 (**Fig. 7e**). It should be noted that the Cu and A components are associated with $\langle 111 \rangle$ fibre, while the Cube and Goss components are connected with $\langle 001 \rangle$ fibre.

4. Discussion

4.1. Deformation texture

The hot rolled starting material (as TMPed 2 material) consisted of a strong texture in which the Rt-Cu component showed the highest intensity and a small fraction of Goss component was also recognized. This is attributed to the occurrence of partial recrystallization through the applied TMP 2. As is seen in **Fig. 2f**, the dislocation density appears to be high after hot deformation. The presence of high volume fraction of low angle grain boundaries (**Fig. 3a**) indicates that the dynamic/static recovery should also be considered as one of the main restoration mechanisms through TMP 2 scheme. The Rt-Cu component is disappeared in the ODF after increasing the tensile strain to 0.15 and replaced by strong Goss and G/B, and weak Goss Twin (GT) and S components. During straining to 0.25, to increase the GT and S components, the texture appears to be developed by deformation twinning and austenite to ϵ -martensite transformation (**Fig. 7c**). By further straining, the GT and S components are gradually decreased while the Cube component is becoming stronger. This gradual transition is accompanied by steady increase of α' -martensite volume fraction and higher kinetics of $\gamma \rightarrow \epsilon \rightarrow \alpha'$ transformation. Decreasing the volume fraction of austenite and increasing the amount of martensite appear to highly influence the austenite texture. By further deformation from 0.35 to 0.4 logarithmic strain, another transition from Cube component to strong G/B, GT and A-

components is realized. The Goss and G/B components of the matrix are not favourable for the transformation. The presence of these components can be attributed to dislocation slip and deformation twinning [24]. The GT component also shows the activation of deformation twinning and its presence even at higher strains confirms the activated TWIP effects at higher strains. The S component carries favourable orientation for the ϵ -martensite formation in plane strain rolling, having the same deformation elements as for mechanical twinning. As is well established any changes in the intensity of S component is in agreement with austenite to ϵ -martensite transformation [2]. According to the present results, the transition of GT and S components into Cube component could lead to an activated TRIP effect. The latter is attributed to the prolonged sequential transformation of $\gamma \rightarrow \epsilon \rightarrow \alpha'$, known as “extended TRIPping effects”. Nezakat et al. [33] showed that the Cube orientation could facilitate the martensite formation with (116)[$\bar{1}\bar{1}0$] orientation. Therefore, it is concluded that the formation of strain-induced martensite can affect the texture of austenite.

The data presented in this paper approve the dominant transformation is being done in $\langle 100 \rangle$ austenite grains (**Fig. 6**) during TRIP process. Based on the data presented in section 3, at strains of 25-35% the formation of α' -martensite and its volume fraction were stimulated in austenite with orientations towards $\langle 100 \rangle$ due to the appearance of Cube texture component. As is seen, the intensity of $\langle 100 \rangle$ orientations are weakened at initial stages of deformation and is transferred toward $\langle 111 \rangle$ orientations through deformation to 25% logarithmic strain. By increasing the strain, the intensity of $\langle 100 \rangle$ orientations along with α' -martensite volume fraction were boosted up. Thus a $\langle 100 \rangle$ transformation texture would be existed and should contribute to the strain hardening behaviour. Moreover, increasing the intensity of A component at interrupted strain of 0.4 is also attributed to the formation of α' -martensite with another variant; this is

different from the α' -martensite that forms in Cube orientation. In **Table 2** the Schmidt factors of some texture components are tabulated. Almost all the texture components possess higher Schmidt factors for twinning than that for dislocation slip. But, the Cube component carries a higher Schmidt factor for dislocation slip. Therefore, the appearance of Cube component can be attributed to the formation of significant amounts of α' -martensite. This is due to the fact that the austenite to martensite transformation would need significant slip of partial dislocations.

4.2. Deformation mechanisms

SFE is the main parameter that can affect the dominant plasticity mechanisms in metals and alloys. In a previous research [22] it was suggested that both TRIP and TWIP effects can occur in steels holding $12 \text{ mJ/m}^2 < \text{SFE} < 20 \text{ mJ/m}^2$. In the present study, the deformation mechanisms were found to be dislocation slip, mechanical twinning and deformation induced ϵ - and α' -martensite.

The present results show that the formation of ϵ -martensite from austenite was continued even up to higher amount of applied strains. But the two-steps (sequential) transformation of $\gamma \rightarrow \epsilon$ and $\epsilon \rightarrow \alpha'$ (i.e. extended TRIPing), is the dominant deformation mechanism at moderate and high strains levels, in the course of present experimental conditions. To better clarify this, as is well-known, the α' -martensite may nucleate at the intersections of deformation bands that can be composed by ϵ -martensite and twins in metastable austenitic steels [34, 36]. The growth of α' -martensite may occur by the nucleation and coalescence of new α' -martensite nuclei repeatedly [35]. Despite the general idea that α' -martensite may form just in low SFE steels [9], however van Tol et al. [37] reported small fractions of α' -martensite ($<1.2\%$) in a TWIP steel during deep drawing by SFE of 50 mJ/m^2 . It can be expected that ϵ -martensite is the main precursor for the $\gamma \rightarrow \alpha'$ transformation in this case [2]. As SFE decreases, the overlapping of stacking faults

becomes more regular, and the nucleation of the α' -martensite becomes easier [38]. Hence, the present results approve that, where the ε -martensite accommodates more strain energy (**Fig. 2f-j**), the α' -martensite formation carries a significant share as deformation mechanism.

The present results indicate that the dislocation slip dominates at lower strains and also continues to play parts up to higher strains. Twinning is also identified as a deformation mechanism in this alloy. Mechanical twinning was observed up to the strain of 0.15 after which its contribution was slightly dropped, but could keep its small share as deformation mechanism up to higher strains (**Fig. 4**). There are two possible explanations for this. At first, at the strains higher than 0.15, the twins might be submerged by the larger quantities of ε -martensite thus could not be detected by EBSD. Secondly, the distortion of austenite could cause such crystal rotations that the twin relationship across their boundaries would be lost [32]. However, the present EBSD images have provided some evidences of deformation twinning at the strain of 0.4 (**Fig. 4d**).

Based on the EBSD results (**Fig. 2b** and **4a**), beyond 15% tensile strain, the transformation of $\gamma \rightarrow \varepsilon$ and deformation twinning are the dominating deformation mechanisms. The ε -martensite and twins form to accommodate excess strain from external loading. While an nuclei of ε -martensite forms by an intrinsic stacking fault on every second $\{111\}$ planes [39], a twin embryo forms by overlapping three stacking faults on successive planes. Then, these mechanisms can occur simultaneously. The KAM map (**Fig. 2g**) also shows that in this deformation level (beyond 15% logarithmic strain), most of the strain is accommodated by austenite phase. The presence of high volume fraction of low angle grain boundaries also approves that the planar dislocation slip is occurred at this level of deformation (**Fig. 3b**). Then, the planar slip of dislocations is another important deformation mechanism in this strain level.

By increasing the tensile strain to 25%, the austenite continues to transform to ϵ -martensite and the deformation twins are increased. Although the interactions of ϵ -martensite and twins with the austenitic phase may differ, but based on Olson et al. results [40], their mechanisms of formation and evolution are in fact similar. By further deformation, the volume fraction of α' -martensite is significantly increased and it appears that two step transformation of $\gamma \rightarrow \epsilon$ and $\epsilon \rightarrow \alpha'$ (extended TRIPing) is the dominant deformation mechanism in this stage (**Fig. 2d and e**).

4.3. Evolution of martensite, dislocation and twin substructure

The strain accommodation in austenite may be carried out by dislocation slip, ϵ -martensite and deformation twins. An ϵ embryo forms by the stacking of single $1/6\langle 112 \rangle$ partials dissociated from $1/2\langle 110 \rangle\{111\}$ perfect dislocations. Therefore, the strain accommodated by ϵ -martensite is a fraction of the strain accommodated by dislocations, because the strain energy of a Shockley partial is $2/3$ of a perfect dislocation energy [41]. Contribution of dislocations to strain accommodation is decreased by increasing the amounts of the twins and ϵ -martensite, promoting the TWIP and TRIP effects respectively, as are shown in **Figs. 2 and 4**. According to **Figs. 2 and 3**, the TRIP effect in dislocation hardening is directly influenced by the ϵ -martensite; α' -martensite affects the hardening response by replacing the deformation bands and by accommodating additional strain.

Gutierrez-Urrutia et al. [29] showed that just the grains with either a highly favourable or unfavourable for twinning follow the Schmidt behaviour. These grains match up to crystals oriented nearby the $\langle 111 \rangle$ and $\langle 001 \rangle$ directions, respectively. This indicates that in the present twin substructure, only grains with $\langle 111 \rangle$ and $\langle 001 \rangle$ orientations follow the Schmidt's behaviour (**Table 2**). The rest of crystals which their orientations are between $\langle 111 \rangle$ and $\langle 001 \rangle$ do not accomplish Schmidt's law under loading. **Figs. 2 and 6** also show that in the present steel,

the local stress concentrations at grain boundaries, like those caused by the impingement of deformation twins formed in a neighbouring grain on a grain boundary, can promote twinning in unfavourably oriented grains. These stresses can be high enough to activate the twin system with the highest Schmidt factor. The growth of the mechanical twins on secondary twin systems may be hindered by the developed twin substructure due to the high stress required to form a secondary twin substructure during tensile deformation [29]. As a result, only primary deformation twins are activated causing a lamellar twin structure.

4.4. Strain partitioning upon deformation

At the early stages of uniform deformation (e.g. logarithmic strain of 15%), the regions with or adjacent to the austenite phase may exhibit higher KAM values (**Fig. 2g**), whereas HCP ϵ phase regions show less notable KAM values. Since the KAM value is associated with the density of geometrically necessary dislocations (GNDs) in the detected region [25], the higher KAM values of the austenite regions suggest a higher density of GNDs and more plastic strains in these zones. The above findings suggest that the plastic strain at this deformation stage was primarily accommodated by the FCC austenite phase. In addition, the EBSD analysis reveals that the strain induced transformation from FCC austenite to HCP ϵ phase and deformation twinning act as the primary deformation mechanism (**Fig. 2** and **Table 1**).

By increasing the strain (e.g. logarithmic strains of 25% and 35%), the strain driven transformation from austenite to ϵ -martensite is replaced by a two-step transformation of $\gamma \rightarrow \epsilon \rightarrow \alpha'$ and the latter remains a prevalent deformation mechanism (**Fig. 2c** and **d**). The deformation induced twinning inside the austenite is also an important deformation mechanism during these loading stages (**Fig. 4b** and **c**) and contributes to the strain hardening of the alloy. The dislocations slip inside the austenite, were also observed during the whole uniform

deformation stages as revealed by EBSD (**Fig. 3**). These observations suggest that the deformation mechanisms in austenite played an important role in the plastic deformation and inter-phase strain accommodation of the alloy at the later uniform deformation stages. In terms of strain partitioning behaviour at medium and late uniform deformation stages, not only the austenite phase regions have higher KAM value, but most HCP and BCC phase regions also exhibit higher KAM values compared to the early uniform deformation stages (**Fig. 2f-i**). This observation suggests that not only the austenite phase partitions the plastic strain but the ϵ and α' phase also accommodate a certain part of the applied strain at these stages via the multiple deformation mechanisms discussed above.

After more straining (e.g. at a local strain of 40%), the two-steps phase transformation proceeded further, leading to a relatively small fraction of retained austenite phase (**Fig. 2e**). It is observed that the martensitic phases are capable of accommodating further plastic straining also at higher strain levels (**Fig. 2j**). Moreover, multiple deformation mechanisms within and/or at the retained austenite may contribute to strain accommodation even at higher strain levels.

5. Conclusion

A comprehensive study was conducted on the evolution of martensitic transformations, twinning, dislocation slip and texture evolution in a high Mn austenitic TRIP-TWIP steel. Deformation mechanisms and strain partitioning behaviour in this austenitic TRIP-TWIP steel during room temperature tensile deformation were examined in detail. Accordingly, the following conclusions can be drawn:

- Martensitic transformations, deformation twinning and planar slip generated a direct effect on the deformation texture of the austenite. Martensitic transformations resulted in

Cube, A and S component textures in austenite. Deformation twinning and dislocation slip could form mainly GT, G/B and Goss textures in the deformed austenite after tensile testing.

- Dislocation slip was realized as the deformation mechanism at all stages of deformation of austenite. Twinning and ϵ -martensite formation played the dominant role at early stages of deformation, while the α' -martensite formation was the most important mechanism by affecting the strain hardening at higher levels of deformation.
- The present TRIP-TWIP steel recorded the development of double fibre texture which is characteristic of FCC materials. A relatively stronger $\langle 111 \rangle$ at early stages of deformation and the strengthening of $\langle 100 \rangle$ fibre through straining were noted parallel to the tensile axis.
- The experimented TRIP-TWIP steel exhibited a dynamic strain partitioning behaviour. At early stages of deformation, the plastic strain was accommodated primarily by the softer and less confined austenite matrix. At later stages of deformation, the martensitic phases partitioned a certain portion of the imposed load. The plastic strains were differently distributed in the austenite, α' - and ϵ -martensite phases. A higher portion of strains was mainly distributed in the softer ϵ -martensite, resulting in higher KAM value regions in the ϵ -martensite during EBSD measurement. The thicker ϵ -martensite could quickly induce α' -martensite due to a smaller strain accumulation caused by the harder α' -martensite during transformation.

Acknowledgments

Professor Pedro E. J. Rivera-Diaz-del-Castillo from department of Engineering in Lancaster University is gratefully acknowledged for proof reading of this paper.

Data Availability Statement

The raw/processed data required to reproduce these findings cannot be shared at this time as the data also forms part of an ongoing study.

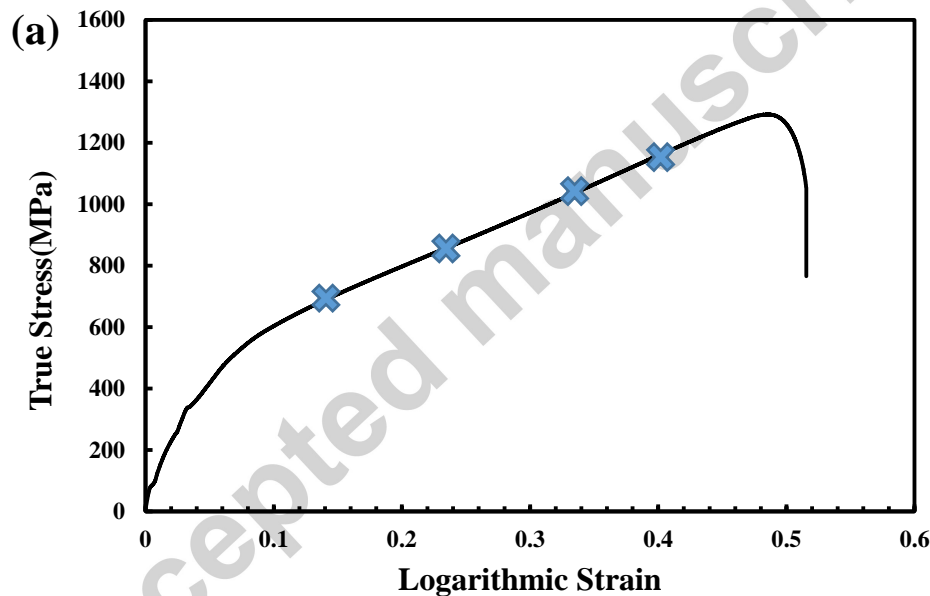
References

- [1] M. Nezakat, H. Akhiani, M. Hoseini, J. Szpunar, Effect of thermo-mechanical processing on texture evolution in austenitic stainless steel 316L, *Mater. Charact.* 98 (2014) 10–17.
- [2] K.A. Ofei, L. Zhao, J. Sietsma, Microstructural Development and Deformation Mechanisms during Cold Rolling of a Medium Stacking Fault Energy TWIP Steel, *J. Mater. Sci. Technol.* 29 (2013) 161–167.
- [3] P. Dastur, A. Zarei-Hanzaki, M.H. Pishbin, M. Moallemi, H.R. Abedi, Transformation and twinning induced plasticity in an advanced high Mn austenitic steel processed by martensite reversion treatment, *Mater. Sci. Eng. A.* 696 (2017) 511–519.
- [4] O. Grässel, L. Krüger, G. Frommeyer, L.W. Meyer, High strength Fe-Mn-(Al, Si) TRIP/TWIP steels development - properties - application, *Int. J. Plast.* 16 (2000) 1391–1409.
- [5] H. Ding, H. Ding, D. Song, Z. Tang, P. Yang, Strain hardening behavior of a TRIP/TWIP steel with 18.8% Mn, *Mater. Sci. Eng. A.* 528 (2011) 868–873.
- [6] R. Ueki, Y. Takagi, N. Tsuchida, K. Shinagawa, Y. Tanaka, T. Mizuguchi, Crystallographic orientation dependence of ϵ martensite transformation during tensile deformation of polycrystalline 30% Mn austenitic steel, *Mater. Sci. Eng. A.* 576 (2013) 14–20.
- [7] A.S. Hamada, L.P. Karjalainen, M.C. Somani, The influence of aluminum on hot deformation behavior and tensile properties of high-Mn TWIP steels, *Mater. Sci. Eng. A.* 467 (2007) 114–124.
- [8] A. Vinogradov, A. Lazarev, M. Linderov, A. Weidner, H. Biermann, Kinetics of deformation processes in high-alloyed cast transformation- induced plasticity/twinning-induced plasticity steels determined by acoustic emission and scanning electron microscopy: Influence of austenite stability on deformation mechanisms, *Acta Mater.* 61 (2013) 2434–2449.
- [9] M. Eskandari, a Zarei-hanzaki, M. Yadegari, N. Soltani, a Asghari, In situ identification of elastic – plastic strain distribution in a microalloyed transformation induced plasticity steel using digital image correlation, *Opt. Lasers Eng.* 54 (2014) 79–87.
- [10] Y.F. Shen, X.X. Li, X. Sun, Y.D. Wang, L. Zuo, Twinning and martensite in a 304 austenitic stainless steel, *Mater. Sci. Eng. A.* 552 (2012) 514–522.

- [11] A. Marandi, N. Haghdadi, M. Eskandari, The prediction of hot deformation behavior in Fe – 21Mn – 2 . 5Si – 1 . 5Al transformation-twinning induced plasticity steel, *Mater. Sci. Eng. A.* 554 (2012) 72–78.
- [12] X. Zhang, T. Sawaguchi, K. Ogawa, F. Yin, X. Zhao, Temperature dependence of intersection reactions of ϵ' martensite plates in an Fe-30Mn-4Si-2Al TRIP/TWIP steel, *J. Alloys Compd.* 577 (2013) S533–S537.
- [13] W. Song, T. Ingendahl, W. Bleck, Control of strain hardening behavior in high-mn austenitic steels, *Acta Metall. Sin. (English Lett.* 27 (2014) 546–555.
- [14] D.T. Pierce, K. Nowag, A. Montagne, J.A. Jiménez, J.E. Wittig, R. Ghisleni, Single crystal elastic constants of high-manganese transformation- and twinning-induced plasticity steels determined by a new method utilizing nanoindentation, *Mater. Sci. Eng. A.* 578 (2013) 134–139.
- [15] T.Y. Liu, P. Yang, L. Meng, F.Y. Lu, Influence of austenitic orientation on martensitic transformations in a compressed high manganese steel, *J. Alloys Compd.* 509 (2011) 8337–8344.
- [16] G.W. Greenwood, R.H. Johnson, The deformation of metals under small stresses during phase transformations, in: *Proc. R. Soc. London A Math. Phys. Eng. Sci.*, The Royal Society, 1965: pp. 403–422.
- [17] I. V Kireeva, Y.I. Chumlyakov, The orientation dependence of γ - α' martensitic transformation in austenitic stainless steel single crystals with low stacking fault energy, *Mater. Sci. Eng. A.* 481 (2008) 737–741.
- [18] B. Petit, N. Gey, M. Cherkaoui, B. Bolle, M. Humbert, Deformation behavior and microstructure/texture evolution of an annealed 304 AISI stainless steel sheet. Experimental and micromechanical modeling, *Int. J. Plast.* 23 (2007) 323–341.
- [19] A. Creuziger, T. Foecke, Transformation potential predictions for the stress-induced austenite to martensite transformation in steel, *Acta Mater.* 58 (2010) 85–91.
- [20] M.-X. Zhang, P.M. Kelly, J.D. Gates, A model of stress induced martensitic transformation in Fe–Ni–C alloy, *Mater. Sci. Eng. A.* 273 (1999) 251–256.
- [21] E. Nagy, V. Mertinger, F. Tranta, J. Sólyom, Deformation induced martensitic transformation in stainless steels, *Mater. Sci. Eng. A.* 378 (2004) 308–313.
- [22] H.E. Sabzi, A.Z. Hanzaki, H.R. Abedi, R. Soltani, A. Mateo, J.J. Roa, The effects of bimodal grain size distributions on the work hardening behavior of a TRansformation-TWinning induced plasticity steel, *Mater. Sci. Eng. A.* 678 (2016) 23–32.
- [23] J. Talonen, H. Hänninen, Formation of shear bands and strain-induced martensite during plastic deformation of metastable austenitic stainless steels, *Acta Mater.* 55 (2007) 6108–6118.
- [24] L. Bracke, K. Verbeken, L. Kestens, J. Penning, Microstructure and texture evolution during cold rolling and annealing of a high Mn TWIP steel, *Acta Mater.* 57 (2009) 1512–1524.

- [25] Z. Li, C.C. Tasan, K.G. Pradeep, D. Raabe, A TRIP-assisted dual-phase high-entropy alloy: Grain size and phase fraction effects on deformation behavior, *Acta Mater.* 131 (2017) 323–335.
- [26] A. Safdel, A. Zarei-Hanzaki, A. Shamsolhodaie, P. Krooß, T. Niendorf, Room temperature superelastic responses of NiTi alloy treated by two distinct thermomechanical processing schemes, *Mater. Sci. Eng. A.* 684 (2017) 303–311.
- [27] M. Ebrahimi, A.Z. Hanzaki, H.R. Abedi, M. Azimi, S. Mirjavdi, Correlating the microstructure to mechanical properties and wear behavior of an accumulative back extruded Al-Mg 2 Si in-situ composite, *Tribol. Int.* (2017).
- [28] Z. MI, D. TANG, Y. DAI, H. WANG, S. LI, Influence of Cold Rolling Reduction on Microstructure and Mechanical Properties of Twip Steel, *Acta Metall. Sin. (English Lett.* 20 (2007) 441–447.
- [29] I. Gutierrez-Urrutia, D. Raabe, Dislocation and twin substructure evolution during strain hardening of an Fe-22 wt.% Mn-0.6 wt.% C TWIP steel observed by electron channeling contrast imaging, *Acta Mater.* 59 (2011) 6449–6462.
- [30] H.-R. Wenk, P. Van Houtte, Texture and anisotropy, *Reports Prog. Phys.* 67 (2004) 1367–1428.
- [31] ASTM, Astm E8, Annu. B. ASTM Stand. i (2008).
- [32] A.A. Saleh, E. V. Pereloma, A.A. Gazder, Microstructure and texture evolution in a twinning-induced-plasticity steel during uniaxial tension, *Acta Mater.* 61 (2013) 2671–2691.
- [33] M. Nezakat, H. Akhiani, S.M. Sabet, J. Szpunar, Electron backscatter and X-ray diffraction studies on the deformation and annealing textures of austenitic stainless steel 310S, *Mater. Charact.* 123 (2017) 115–127.
- [34] A.A. Al-Joubori, C. Suryanarayana, Synthesis and stability of the austenite phase in mechanically alloyed Fe–Cr–Ni alloys, *Mater. Lett.* 187 (2017) 140–143.
- [35] S. Ackermann, S. Martin, M.R. Schwarz, C. Schimpf, D. Kulawinski, C. Lathe, S. Henkel, D. Rafaja, H. Biermann, A. Weidner, Investigation of Phase Transformations in High-Alloy Austenitic TRIP Steel Under High Pressure (up to 18 GPa) by In Situ Synchrotron X-ray Diffraction and Scanning Electron Microscopy, *Metall. Mater. Trans. A.* 47 (2016) 95–111.
- [36] H.N. Han, C.G. Lee, D.W. Suh, S.J. Kim, A microstructure-based analysis for transformation induced plasticity and mechanically induced martensitic transformation, *Mater. Sci. Eng. A.* 485 (2008) 224–233.
- [37] R.T. Van Tol, J.K. Kim, L. Zhao, J. Sietsma, B.C. De Cooman, α' -Martensite formation in deep-drawn Mn-based TWIP steel, *J. Mater. Sci.* 47 (2012) 4845–4850.
- [38] K.-T. Park, K.G. Jin, S.H. Han, S.W. Hwang, K. Choi, C.S. Lee, Stacking fault energy and plastic deformation of fully austenitic high manganese steels: Effect of Al addition, *Mater. Sci. Eng. A.* 527 (2010) 3651–3661.

- [39] E.I. Galindo-Nava, P.E.J. Rivera-Díaz-del-Castillo, Understanding martensite and twin formation in austenitic steels: A model describing TRIP and TWIP effects, *Acta Mater.* 128 (2017) 120–134.
- [40] G.B. Olson, M. Cohen, Kinetics of strain-induced martensitic nucleation, *Metall. Mater. Trans. A.* 6 (1975) 791–795.
- [41] H. Fujita, S. Ueda, Stacking faults and fcc (γ) \rightarrow hcp (ϵ) transformation in 188-type stainless steel, *Acta Metall.* 20 (1972) 759–767.
- [42] R. Smallman, D. Green, The dependence of rolling texture on stacking fault energy, *Acta Metall.*, 12 (1964), pp. 145-154.
- [43] R.K. Ray, Rolling textures of pure nickel, nickel-iron and nickel-cobalt alloys, *Acta Metall. Mater.*, 43 (1995), pp. 3861-3872.



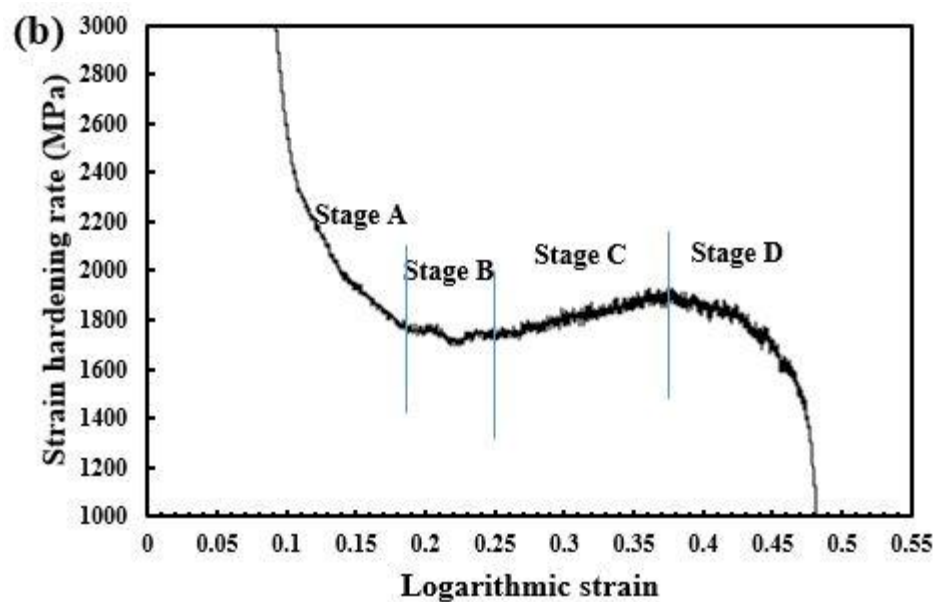


Fig. 1. (a) The true stress vs. Logarithmic strain curve, and (b) the strain hardening rate behavior of the experimented TMPed 2 TRIP-TWIP steel.

(c)

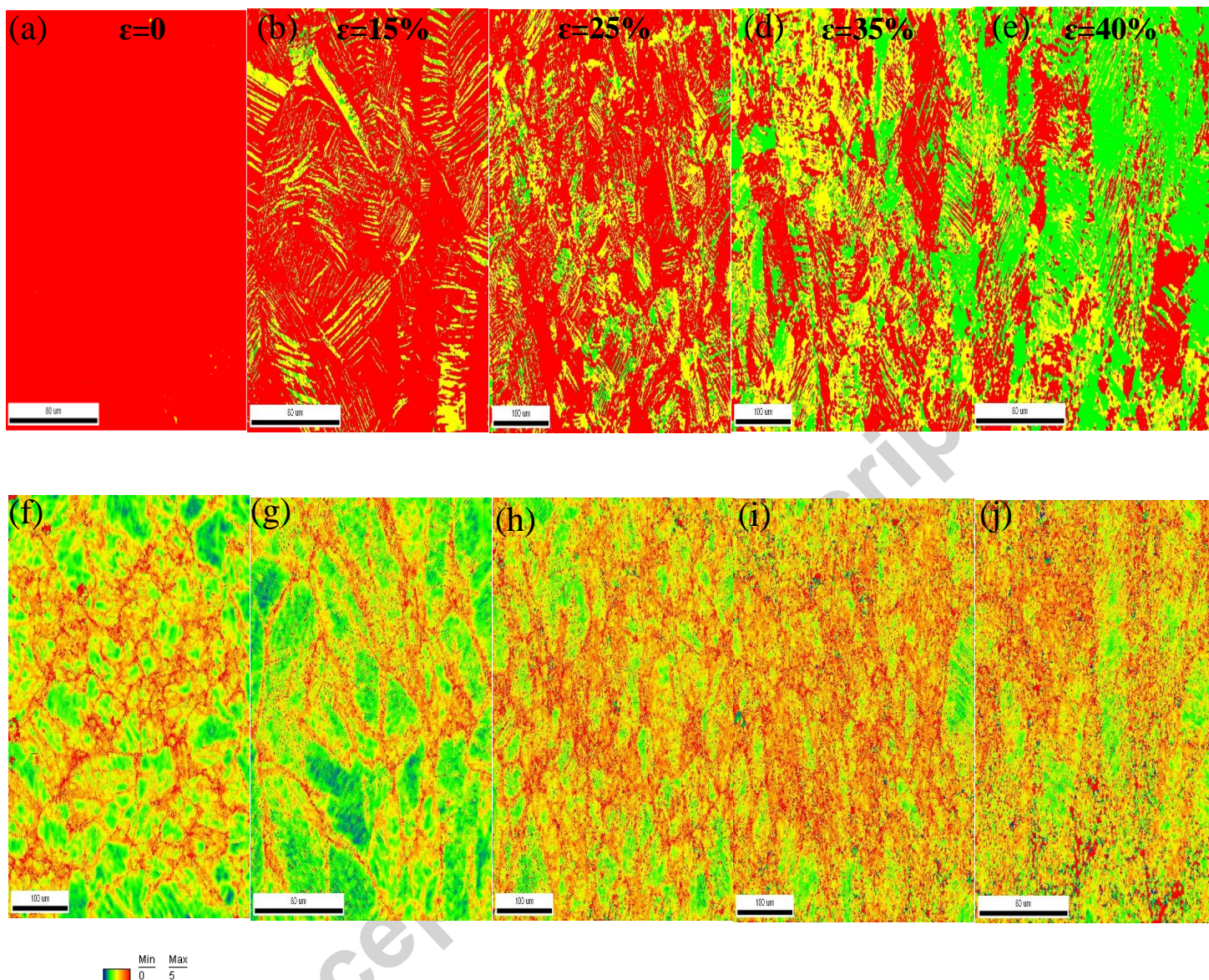


Fig. 2. (a-e) The EBSD phase images, and (f-j) the KAM maps of TMPed 2 material further to applying tensile deformations to interrupted strain levels of 0, 15%, 25%, 35% and 40%, respectively. In the phase maps, the red color refers to austenite, yellow and green refers to ϵ and α -martensite, respectively.

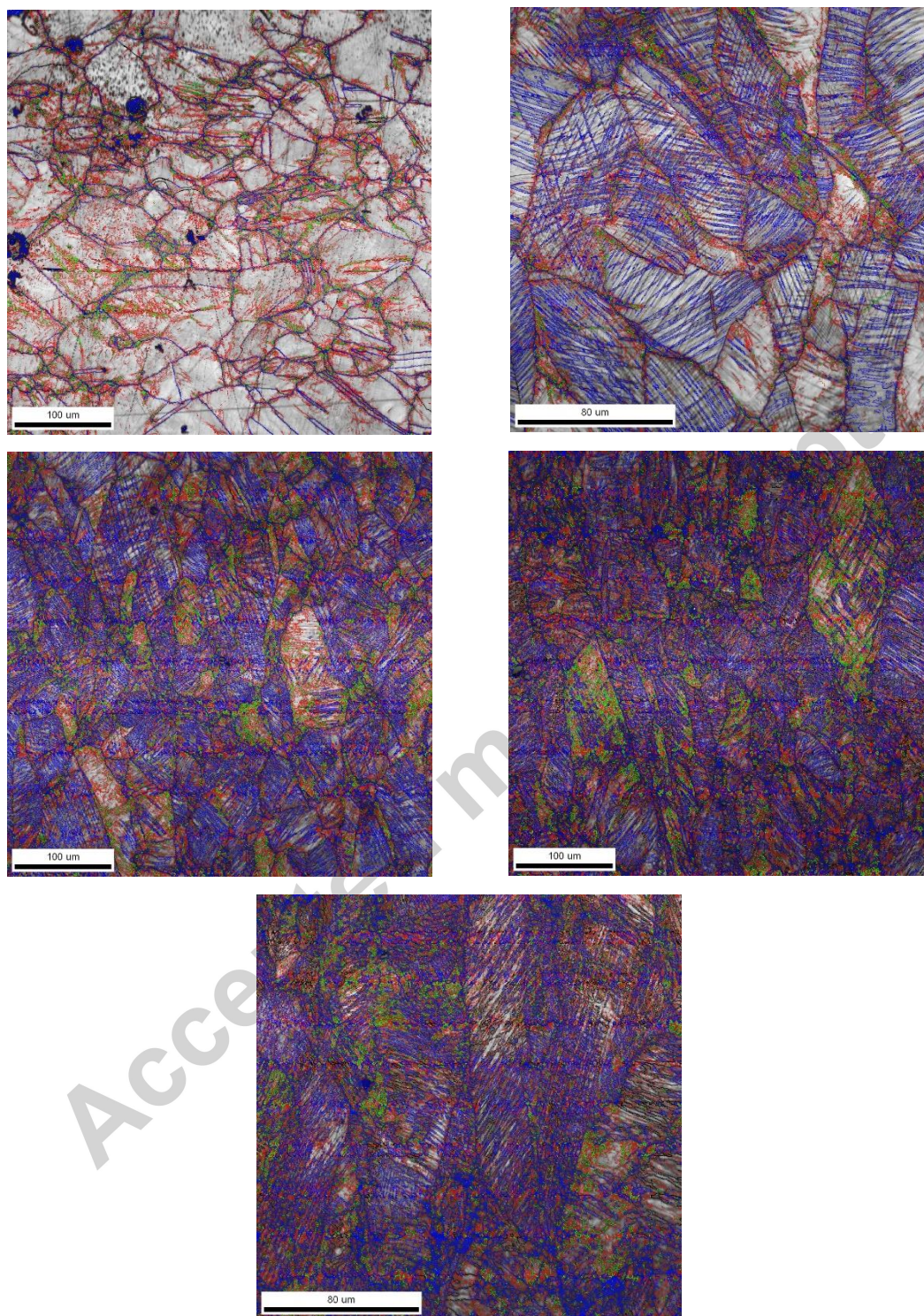


Fig. 3. The IQ+GB maps at tensile strains of (a) 0%, (b) 15%, (c) 25%, (d) 35% and (e) 40%. Low angle grain boundaries (between 2-5 degrees) are shown in red, moderate angle grain boundaries (between 5-15 degrees) in green and high angle grain boundaries (more than 15 degrees) in blue.

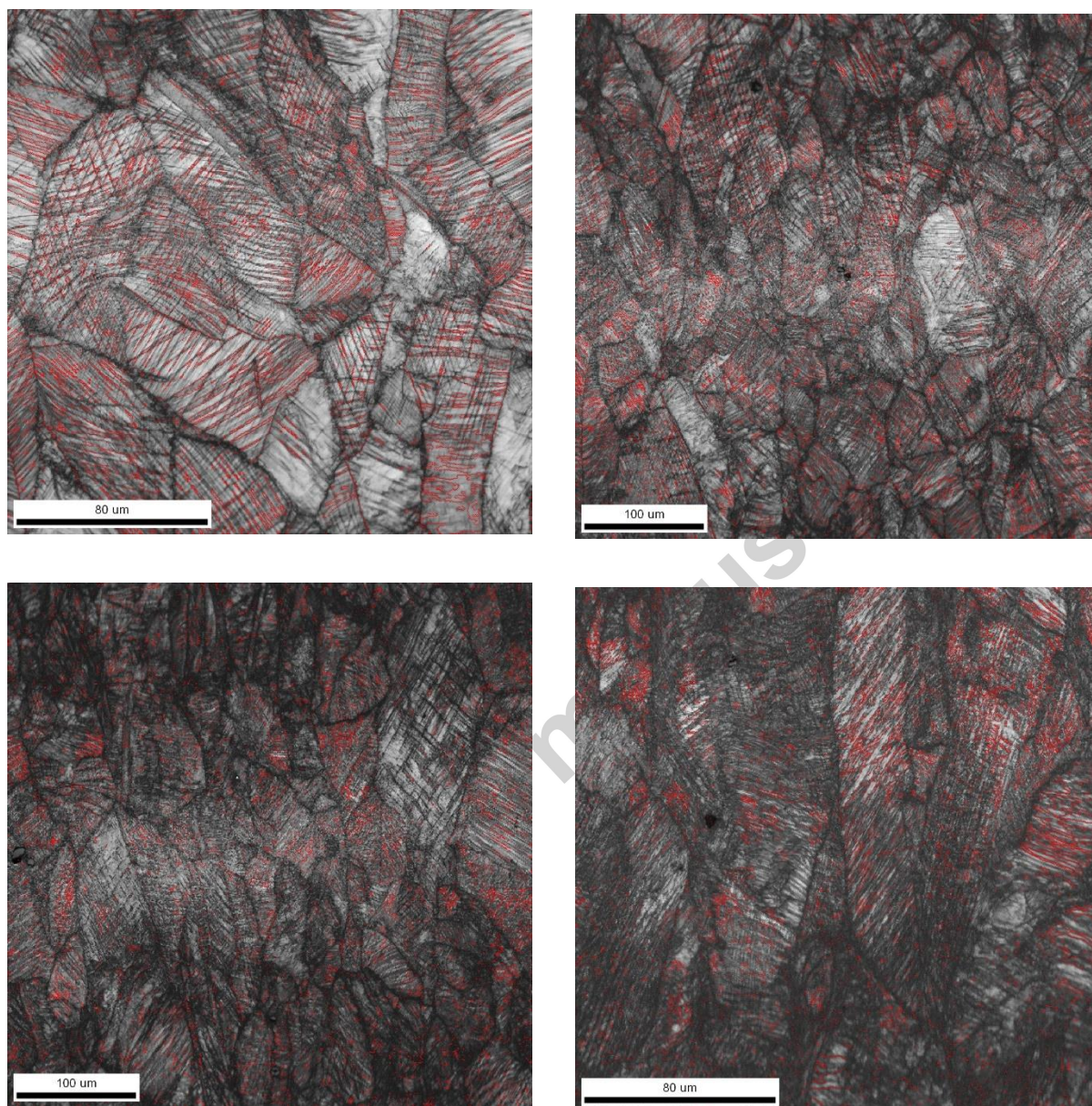
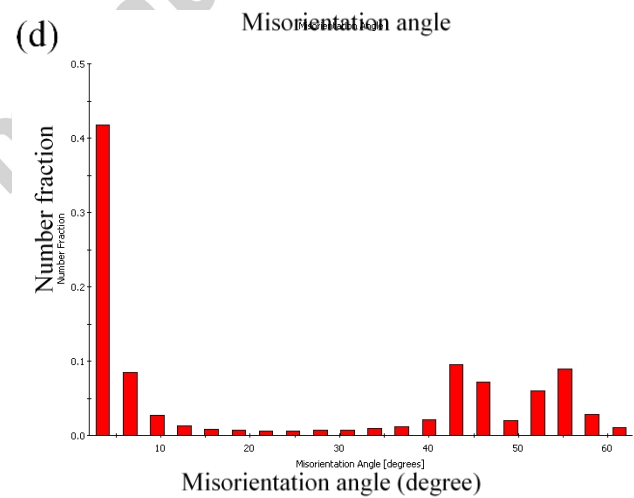
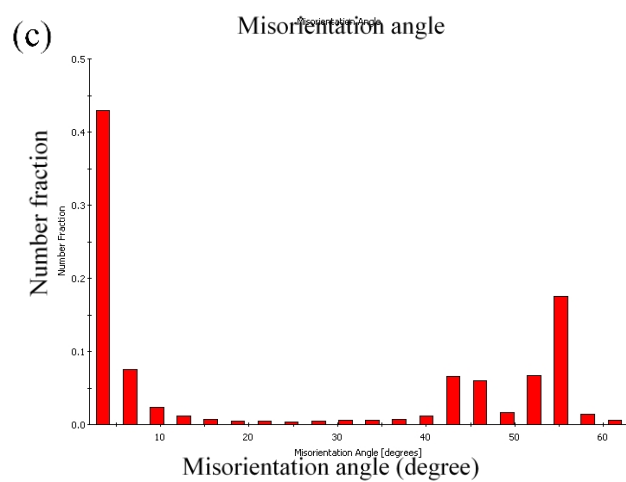
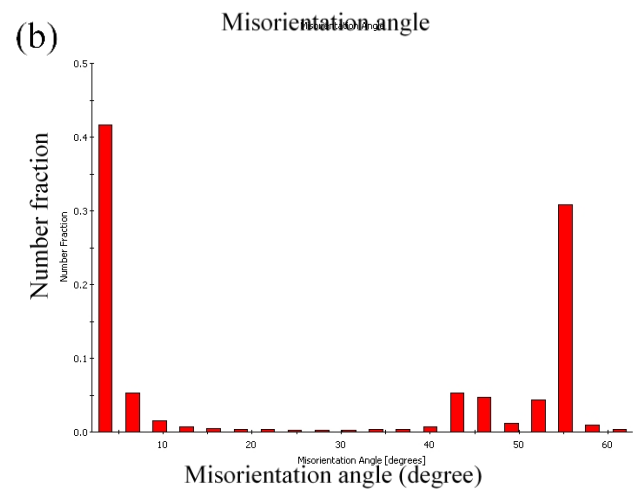
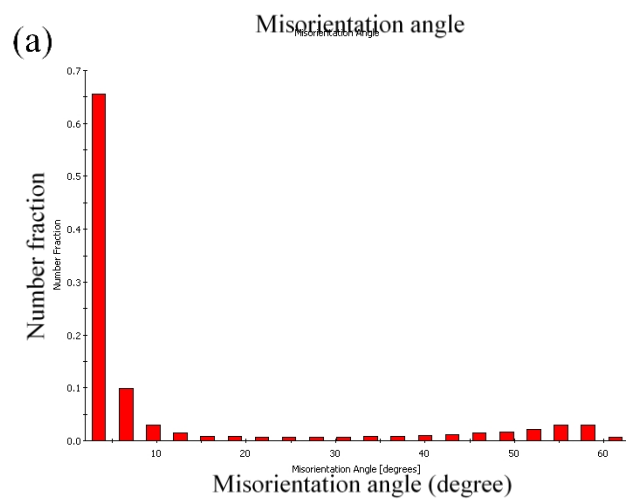


Fig. 4. The IQ map superimposed by twin boundary map of the tensile strained specimens to logarithmic strain of (a) 0.15, (b) 0.25, (c) 0.35 and (d) 0.4.



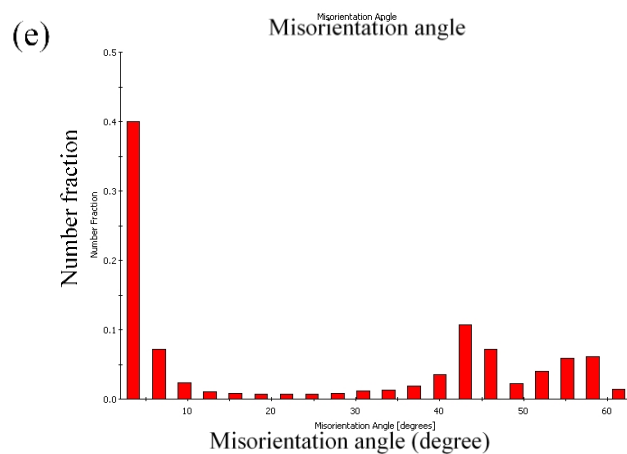


Fig. 5. The change in misorientation angle distribution in the specimens deformed up to the tensile strains of: (a) 0%, (b) 15%, (c) 25%, (d) 0.35 and (e) 0.4.

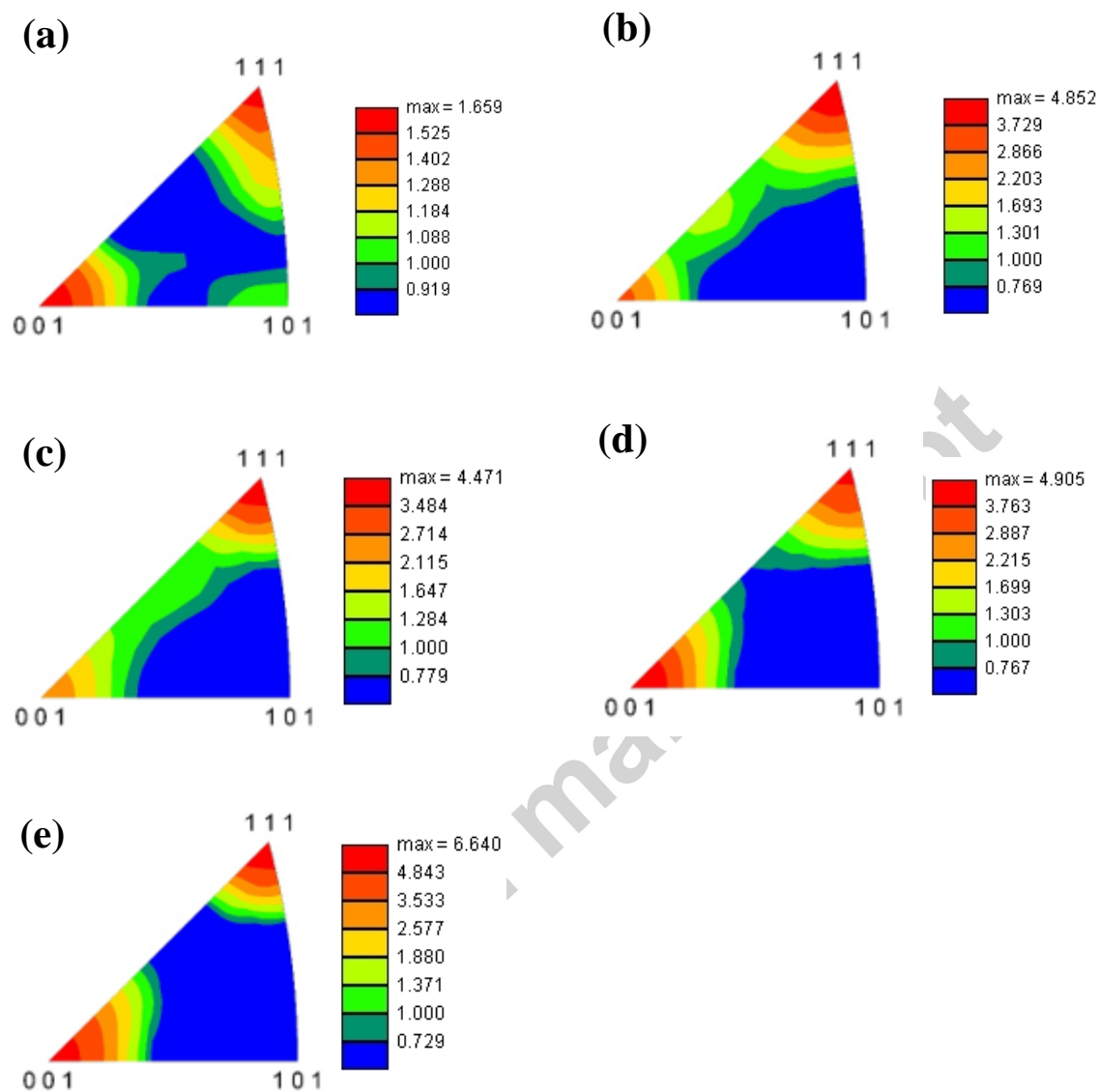


Fig. 6. The IPFs along the TA direction in the specimens holding different states: (a) as hot rolled (TMPed 2 material), and tensile deformed to (b) 0.15, (c) 0.25, (d) 0.35 and (e) 0.4 logarithmic strain.

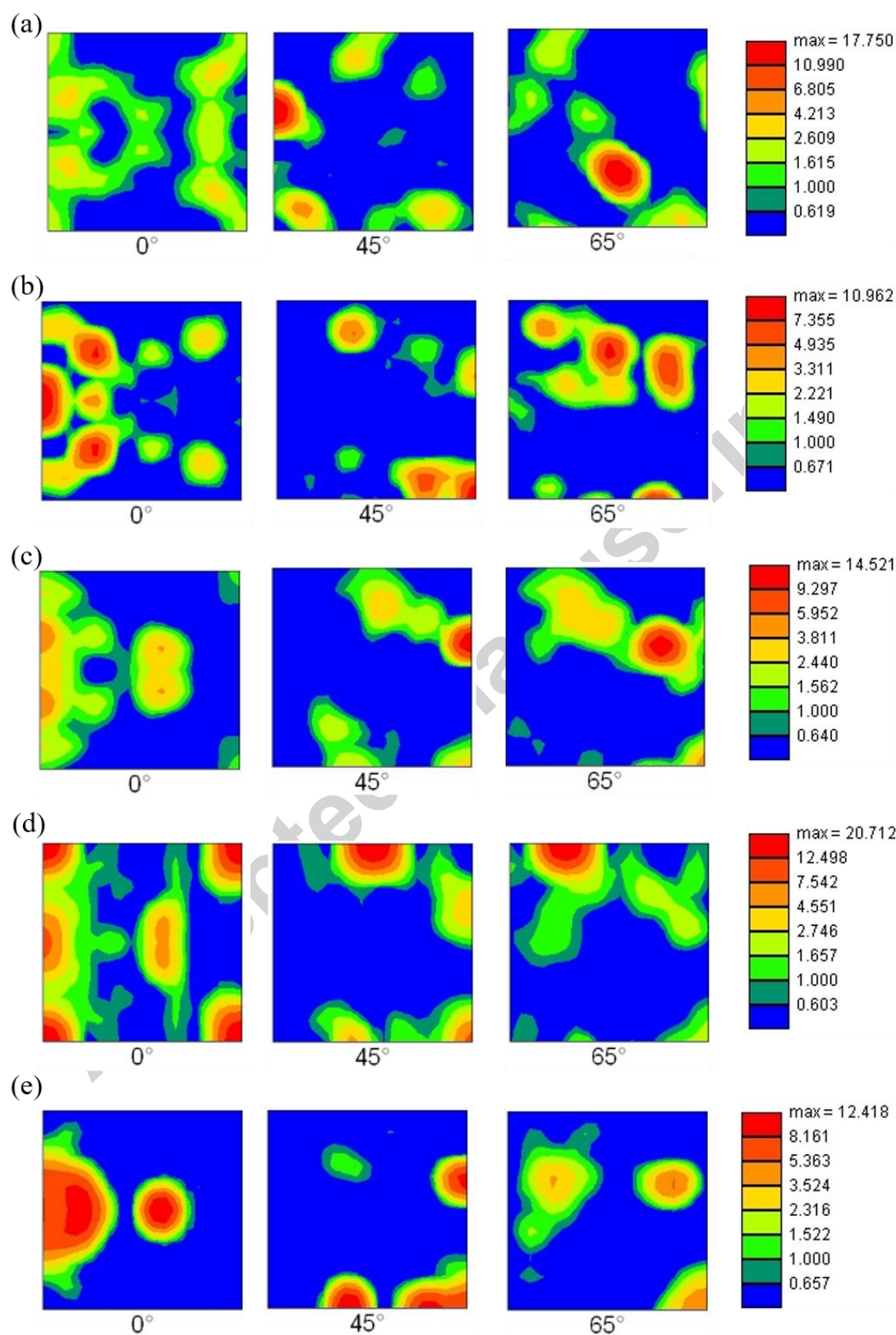


Fig. 7. The ODF sections ($\Phi_2 = 0^\circ, 45^\circ$ and 65°) of the bulk experimental material macro-texture at interrupted tensile strains of (a) 0%, (b) 15%, (c) 25%, (d) 35%, (e) 40%.

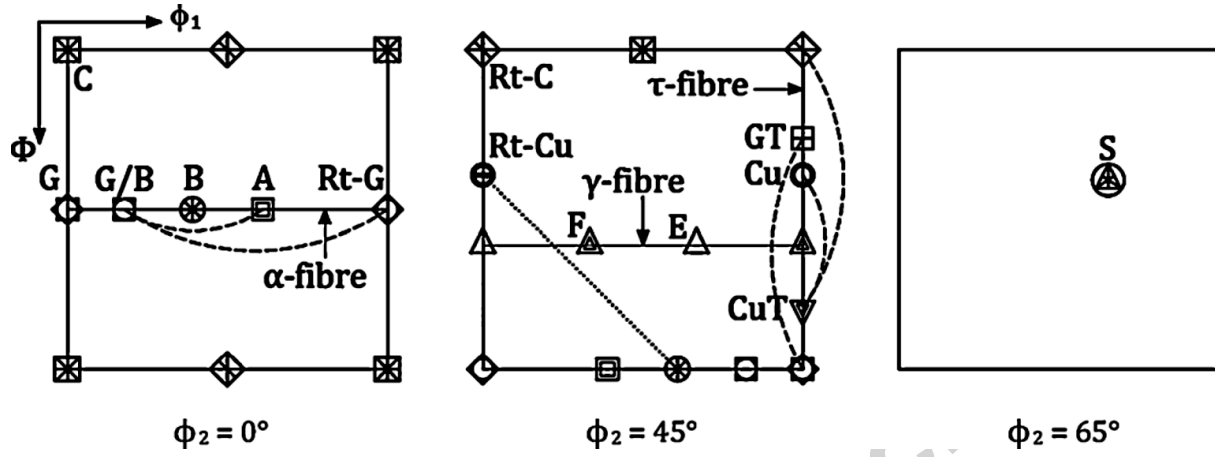
















Fig. 8. A schematic representation of the important texture components in FCC materials [33].

Table 1. Area fraction of austenite, ϵ -martensite and α' -martensite from EBSD analysis at different strain levels.

Strain	Austenite (%)	ϵ -martensite (%)	α' -martensite (%)
0	100	0	0
0.15	80	17	3
0.25	66	27	7
0.35	43	36	21
0.4	30	25	45

Table 2. Euler angles and Miller indices for common texture components in f.c.c metals and alloys [33].

Texture components	Symbol	{hkl}<uvw>	Euler angles	Fiber	Schmidt's factor	
					Slip Twinning	
Cube (C)		{001}<100>	45/0/45	-	0.41 0.24	
Goss (G)		{110}<001>	90/90/45	α/τ	0.41 0.47	
G/B		{110}<115>	74/90/45	α		
Brass (B)		{110}<112>	55/90/45	α/β	0.41 0.47	
A		{110}<111>	35/90/45	α		
Rotated Goss (Rt-G)		{011}<011>	0/90/45	α	0.41 0.47	
Rotated Cube (Rt-C)		{001}<110>	90/0/45	τ		
Goss Twin (GT)		{113}<332>	90/25/45	τ		
Copper (Cu)		{112}<111>	90/35/45	τ/β	0.4	0.4
Copper Twin (CuT)		{552}<115>	90/74/45	τ		
S		{123}<634>	59/37/63	β	0.46	0.47
Rotated Copper (Rt-Cu)		{112}<011>	0/35/45	-		

F		$\{111\}\langle 112\rangle$	90/55/45	γ/τ	0.27	0.31
E		$\{111\}\langle 011\rangle$	60/55/45	γ	0.27	0.31

Accepted manuscript